JOURNAL OF PROPULSION AND POWER
Vol. 16, No. 5, September–October 2000

Fluid Circuit Model for Long-Bearing Squeeze Film Damper Rotordynamics

Paul A. Schallhorn,* David A. Elrod,† David G. Goggin,‡ and Alok K. Majumdar§
Sverdrup Technology, Inc., Huntsville, Alabama 35806

Results of a rotordynamic analysis of a long-bearing squeeze film damper using a fluid circuit approach are presented. A series of nodes and branches represent the geometry of the flow circuit. The mass and momentum conservation equations are solved to predict the pressure distribution in the squeeze film. The motion of the bearing is simulated by injection/removal of mass at the nodes. The modeling methodology is benchmarked against published experimental long-bearing squeeze film damper test results. The model provides good agreement with the experimental damping coefficient.

Nomenclature

C = squeeze film damper radial clearance (difference in radii)
C_p = pressure conversion factor, $\mu\omega R^2/C^2$
C_{tt} = dimensionless direct damping coefficient, $-f_t/\varepsilon$
D_{rr} = dimensionless direct inertia coefficient, f_r/ε
d = damper journal diameter
e = dynamic eccentricity (orbit radius)
L = damper journal length
$\dot{m}$ = mass-flow rate
p = local pressure within the squeeze film region
p_{ref} = reference pressure, $C_p Re = \rho(R\omega)^2$
R = damper journal radius
Re = Reynolds number, $\rho\omega C^2/\mu$
r = radial coordinate
z = axial coordinate
ε = eccentricity ratio (dimensionless orbit radius), e/C
θ = circumferential coordinate
μ = fluid absolute viscosity
ρ = fluid density
τ_f = shear stress
ω = frequency of damper journal (whirl frequency)

Introduction

SQUEEZE film dampers (SFD) have been used to provide damping in high-speed rotating machinery with rolling element bearings for years. Extensive research has been performed both experimentally and analytically to examine the effects of geometry, cavitation, Reynolds number, etc., on SFD pressures and forces. The experimental work of Jung et al.[1,2] examined the pressure distributions and force coefficients for an SFD executing circular-centered orbits for both open-ended (short-bearing) and partially sealed (long-bearing) configurations. Analytical, circular-centered orbit, SFD models have been published for a variety of Reynolds numbers for both long-bearing (axial flow neglected) and short-bearing (circumferential flow neglected) assumptions. Analytical work by San Andres,[3] San Andres and Vance,[4–6] and Tichy[7–9] addressed the effects of fluid inertia on both short- and long-bearing SFDs and the effect of turbulence on short-bearing SFDs.

Presented as Paper 98-3683 at the AIAA/ASME/SAE/ASEE 34th Joint Propulsion Conference, Cleveland, OH, 13–15 July 1998; received 19 December 1998; revision received 31 August 1999; accepted for publication 20 September 1999.

*Engineer, Engineering Directorate, 620 Discovery Drive. Senior Member AIAA.
†Senior Engineer, Space Transportation Directorate, 620 Discovery Drive.
‡Lead Engineer, Space Transportation Directorate, 620 Discovery Drive.
§Senior Engineer, Space Transportation Directorate, 620 Discovery Drive. Member AIAA.

This paper presents the application of a fluid network code to the analysis of fluid forces in a noncavitating, long-bearing SFD. Comparisons of the analytical predictions to the experimental work of Jung et al.[2] are presented. This work provides the foundation for the investigation of statically eccentric, large-orbit SFD forces and rotordynamic coefficients.

Fluid Flow Code

A general purpose, one-dimensional, network-flow-analysis computer code was chosen as the platform for SFD modeling.[10] The code uses a series of nodes and branches to define a flow network. Nodes are positions within the network where fluid properties (pressure, density, etc.) are either known or calculated. Branches are the portions of the flow network where flow conditions (geometry, flow rate, etc.) are known or calculated.

Governing Equations

The governing equations used in this analysis are the continuity and one-dimensional momentum equation. Equations (1) and (2) are the steady-state governing equations used in the analysis. Equation (1) is the steady-state continuity equation for the flow into a node, where

$$\sum \dot{m}_{\text{in}}$$

is the summation of flow into a node through the branches connecting to it,

$$\sum \dot{m}_{\text{out}}$$

is the summation of flow out of a node through the branches connecting to it, and $\dot{m}_{\text{source}}$ is a mass source term (which accounts for any other mass flow into or out of the node). Equation (2) represents the conservation of momentum for a branch in the flow network, where Δp is the pressure difference across the branch, $A_{\text{Cross section}}$ is the cross-sectional area, τ_f is the shear stress, A_{Shear} is the shear area, and $\text{mom}_{\text{Source}}$ is a momentum source, that is, any other force term not accounted for by the two previous terms. The momentum equation equates the sum of the pressure drop and any momentum source with the shear stress, obtained from an empirically derived friction factor:

$$\sum \dot{m}_{\text{in}} - \sum \dot{m}_{\text{out}} + \dot{m}_{\text{source}} = 0 \tag{1}$$

$$-\Delta p A_{\text{Cross section}} - \tau_f A_{\text{Shear}} + \text{mom}_{\text{Source}} = 0 \tag{2}$$

Equations (1) and (2) are solved by a simultaneous solution iterative scheme (Newton–Raphson scheme) to obtain the branch flow rates and node pressures.

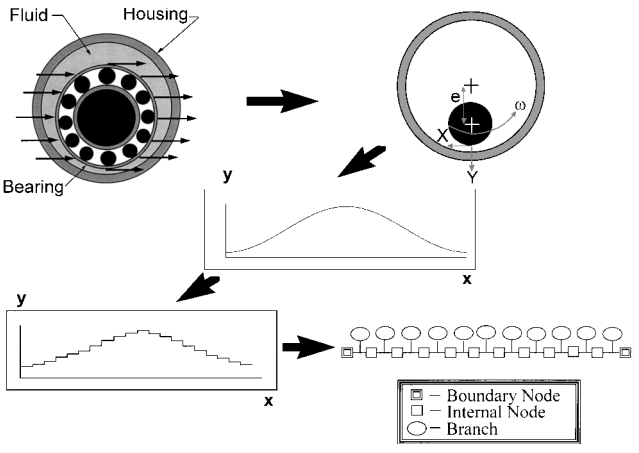

Fig. 1 SFD modeling.

Steady-State, Long-Bearing SFD Modeling

The modeling used in the analysis is shown schematically in Fig. 1. In the analysis, the bearing is unwrapped, and curvature is neglected because the clearance-to-radius ratio is small ($\sim 1/40$). Because the bearing is unwrapped, there exists a periodic situation at the ends, and it must be modeled using a periodic boundary condition. To simulate this periodic boundary, conditions at the boundary nodes must be the same, that is, $p|_0 = p|_{2\pi}$, $\partial p/\partial\theta|_0 = \partial p/\partial\theta|_{2\pi}$, and $\dot{m}_0 = \dot{m}_{2\pi}$. The pressure at the boundary nodes is established in boundary conditions; however, the slope of the pressure and the mass flow into/out of these nodes need to be calculated/supplied as output from the results to verify proper modeling of periodicity. The fluid is considered to be perfectly incompressible, so the absolute pressure values are of no significance in the calculation of the flowfield. Furthermore, fluid film forces in a SFD are due to pressure differences from point to point. Based on the perfectly incompressible assumption, the pressure at these boundary nodes can be arbitrarily set to zero. To convert the time-dependent geometry, that is, time-varying clearances, to steady state, a moving coordinate system is used with the origin fixed at the point of minimum clearance. This coordinate transformation is only valid for circular-centered orbits and is a commonly used technique by other investigators, including San Andres and Vance[6] and Tichy.[7]

The coordinate transformation introduces a term that does not fit into the standard form of the momentum equation. To illustrate, consider the two-dimensional Navier–Stokes equation. Equation (3) is the Navier–Stokes equation in a fixed coordinate system, where X is tangent to the bearing and Y is normal to the bearing. At time $= 0$, the origin of the coordinate system coincides with the position of minimum clearance. For the moving-coordinate system, the unsteady term drops out, x is tangent to the bearing, y is normal to the bearing, and the coordinate system is moving with the minimum gap (moving at a speed of ωR). Therefore, the transformed coordinate system is given by Eqs. (4) and (5). Equation (6) presents the moving coordinate system form of the Navier–Stokes equation. The nonstandard term, therefore, is the $R\omega(\partial\bar{u}/\partial x)$ term [from Eq. (6)]:

$$\frac{\partial \bar{U}}{\partial t} + U\frac{\partial \bar{U}}{\partial X} + V\frac{\partial \bar{U}}{\partial Y} = -\frac{1}{\rho}\nabla p + \nu\left(\frac{\partial^2 \bar{U}}{\partial X^2} + \frac{\partial^2 \bar{U}}{\partial Y^2}\right) \tag{3}$$

$$x = X - R\omega t \tag{4}$$

$$y = Y \tag{5}$$

$$u\frac{\partial \bar{u}}{\partial x} + R\omega\frac{\partial \bar{u}}{\partial x} + v\frac{\partial \bar{u}}{\partial y} = -\frac{1}{\rho}\nabla p + \nu\left(\frac{\partial^2 \bar{u}}{\partial x^2} + \frac{\partial^2 \bar{u}}{\partial y^2}\right) \tag{6}$$

To model this additional term, a momentum source is introduced into the momentum equation. The motion of the bearing is simulated by the injection/removal of fluid at the internal nodes in the form of a mass source. The value of the mass source is given by Eq. (7), where the normal velocity component of the rotor is given by Eq. (8). The net injection of mass is zero [Eq. (9)]:

$$\dot{m}_{\text{source}} = \rho A_{\text{normal}} v_{\text{normal}} \tag{7}$$

$$v_{\text{normal}} = (c\varepsilon\omega)\cos(x/R) \tag{8}$$

$$\sum_{i=1}^{n} \dot{m}_{\text{source}_i} = 0 \tag{9}$$

where, n is the total number of nodes.

For rotordynamics applications, the pressure distribution of the fluid circuit model is integrated to obtain the radial and tangential forces of Eqs. (10) and (11):

$$F_r = \int_0^{2\pi} pA_{\text{normal}}\cos\theta\,\mathrm{d}\theta \tag{10}$$

$$F_t = \int_0^{2\pi} pA_{\text{normal}}\sin\theta\,\mathrm{d}\theta \tag{11}$$

In a dimensionless form, the radial and tangential forces are calculated using Eqs. (12) and (13), where C_p is the pressure coefficient:

$$f_r = \int_0^{2\pi} \frac{p}{C_p}\cos\theta\,\mathrm{d}\theta \tag{12}$$

$$f_t = \int_0^{2\pi} \frac{p}{C_p}\sin\theta\,\mathrm{d}\theta \tag{13}$$

In rotordynamic models, these force components are represented by rotordynamic coefficients. These coefficients are analogous to the mass, damping, and stiffness terms for a spring–mass–damper system. For an uncavitated squeeze film damper, the only two coefficients that occur are a radial inertia (or added mass) term D_{rr} and a circumferential damping term C_{tt}. To compare with published experimental results,[2] the damping and inertia coefficients are normalized by the eccentricity ratio and pressure coefficient, Eqs. (14) and (15). Equation (14) is the nondimensional circumferential damping coefficient and Eq. (15) is the nondimensional radial inertia coefficient:

$$C_{tt} = -f_t/\varepsilon \tag{14}$$

$$D_{rr} = f_r/\varepsilon \tag{15}$$

SFD Experimental Benchmark

The experimental results of Jung et al.[2] were used to validate the modeling methodology. The experimental work simulated a long-bearing SFD by using an O-ring seal on one side of the bearing and a serrated piston ring on the other side of the bearing to limit axial flow. A Reynolds number of 49.0 and an eccentricity ratio of 0.82 were chosen for comparison as the data indicate that cavitation was not present.

Results

Basic Model

Figure 2 shows the pressure profile of the initial 20-node, 19-branch SFD model compared with the Jung et at.[2] experimental results. The pressure has been nondimensionalized using Eq. (16) for comparison with the Jung et al. published data:

$$\frac{p}{p_{\text{ref}}} = \frac{p}{C_p Re} = \frac{p}{\rho R^2\omega^2} \tag{16}$$

To verify periodicity, it was necessary to confirm that the mass-flow rate into the two boundary nodes were equal as well as to calculate that the slope of the pressure at the two boundary nodes were equal. The code output provides the mass-flow rate and pressure. Results for the basic model show that the mass-flow rates at the boundary

Table 1 Dimensionless benchmark rotordynamic coefficient comparison

Parameter	C_{tt}	D_{rr}
45-node prediction	88.78	10.71
Jung et al. experimental result[2]	~84.6	~29.5

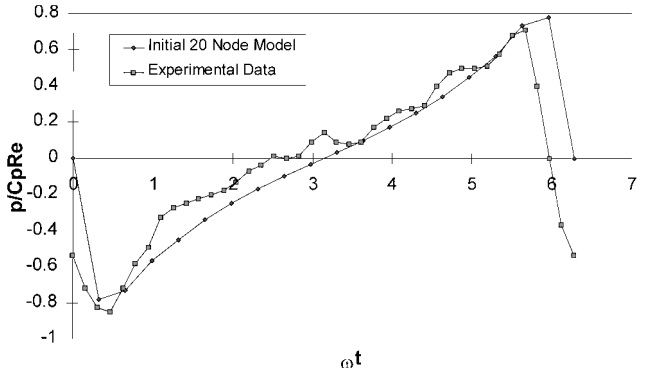

Fig. 2 Initial 20-node model dimensionless SFD pressure profile prediction with the Jung et at.[2] data overlay.

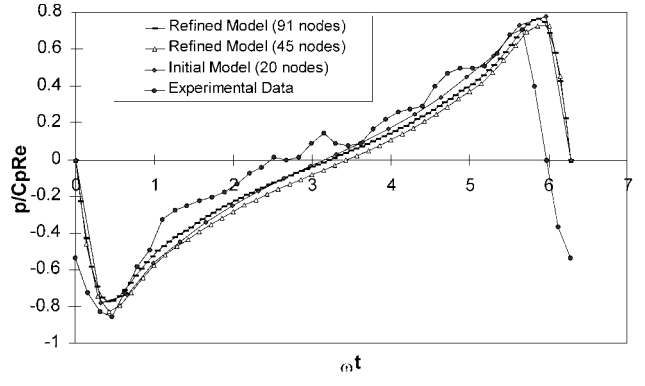

Fig. 3 Expanded models dimensionless SFD pressure profile predictions with the Jung et al.[2] data overlay.

nodes are the same. The pressure gradient at the boundary nodes, which was calculated from the code output, differed by less than 0.01%. These results verify that the periodic boundary condition was adequately modeled using the approach outlined earlier.

The predicted pressure profile follows the same trend as the experimental data; however, there is a phase shift of approximately 18 deg between the prediction and the experimental results. This phase shift is due to the imposed periodic boundary condition at the minimum gap position in the squeeze film region. The initial model was expanded to examine the effect of a grid; two additional models were constructed, a 45-node and a 91-node model. The dimensionless pressure profiles for all three models along with the experimental data are presented in Fig. 3. The rotordynamic coefficients corresponding to the 45-node model are presented in Table 1, along with the Jung et al.[2] experimentally derived coefficients. As Table 1 indicates, the damping coefficient C_{tt} predicted by the code agrees well with the experimental values, whereas the code's prediction of the inertia coefficient D_{rr} is poor. The difference between the predicted and experimental inertia coefficients is due to the phase shift noted earlier.

Parametric Studies

A set of parametric studies was performed on the basic model to verify key requirements for SFD modeling. The first parametric study examined the variation of the pressure profile with SFD clearance. The second parametric study examined the variation of the pressure profile with the rotational speed of the rotor ω. In one case the clearance was cut to 50% of the original value. In the other case the running speed was set at 200% of the original value. The results of this parametric study are shown in Fig. 4. The pressure profile for these cases is proportional to the inverse cube of the clearance for case 1 and is linearly proportional with the running speed for the second case. These results agree with theory.[11]

The third study examined the effect of Reynolds number on the rotordynamic coefficients. Figures 5 and 6 show the variation of predicted rotordynamic coefficients with Reynolds number. The results are compared with the Jung et al.[2] experimental results and their predictions using an uncavitated model. Figure 5 shows that the present predictions agree well with the experimental damping coefficient, whereas the Jung et al. uncavitated model does not predict the increase in damping as Reynolds number increases. Figure 6 shows that the inertia coefficient of the present analysis does not compare favorably with the experimental results, although the Jung et al. prediction does.

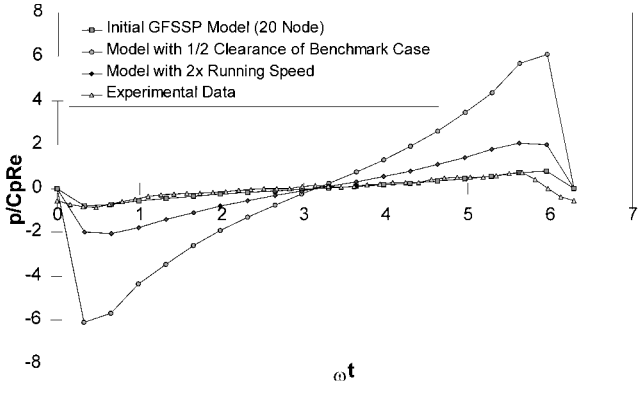

Fig. 4 Clearance and speed parametric study pressure profile predictions with the Jung et al.[2] data overlay.

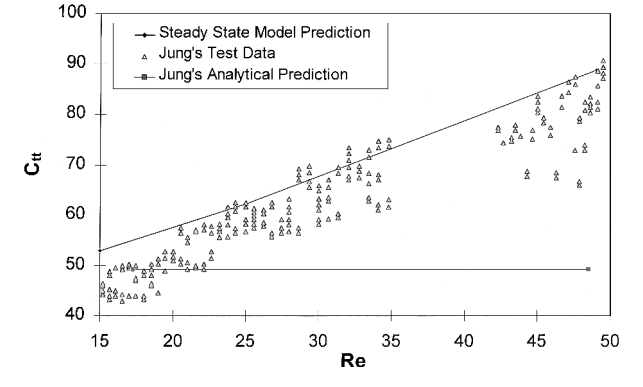

Fig. 5 Dimensionless damping coefficient predictions with the Jung et al.[2] experimental and analytical results.

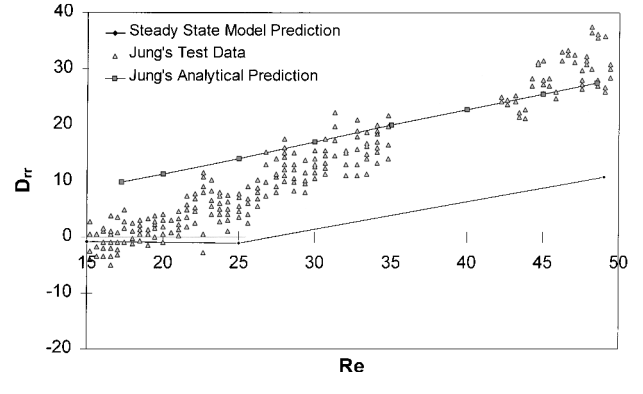

Fig. 6 Dimensionless inertia coefficient predictions with the Jung et al.[2] experimental and analytical results.

Conclusions

A long-bearing SFD rotordynamic analysis has been developed and successfully implemented. The approach uses a general one-dimensional fluid flow code in which shear stress is calculated using friction factors. The normal velocity of the rotor is simulated by the injection/removal of mass (corresponding to the velocity) at various discrete locations within the flow network. Results have been compared with experimental results. The predicted pressure profile compared favorably to the experimental data, except for an approximately 18-deg phase shift. A set of parametric studies was conducted that validated the modeling technique. In the first two studies, clearance and running speed were varied independently. The results of this study agree with published theory. The third study varied the operational Reynolds number to compare rotordynamic coefficient predictions with experimentally derived coefficients. The damping coefficients predicted over a range of Reynolds numbers agree well with the experimentally derived damping coefficients, unlike prior predictions. However, the inertia coefficient does not compare favorably with the experimentally derived values. It is believed that this discrepancy is due to the aforementioned phase shift.

An unsteady, long-bearing SFD analysis using the basic approach presented here will be constructed to model statically eccentric SFDs. The approach will allow for the variation of geometry within the flow paths (branches) to model the motion of the rotor instead of using mass injection.

Acknowledgments

The work was performed for the NASA Marshall Space Flight Center under Task Directive 611-022 for Contract NAS8-40836 with Eric Earhart as the Task Initiator. The authors would like to acknowledge the support of Steven Ryan of NASA Marshall Space Flight Center and Robert LeMaster of Sverdrup Technology.

References

[1] Jung, S. Y., San Andres, L. A., and Vance, J. M., "Measurements of Pressure Distributions and Force Coefficients in a Squeeze Film Damper Part I: Fully Open Ended Configuration," *Tribology Transactions*, Vol. 34, No. 3, 1991, pp. 375–382.

[2] Jung, S. Y., San Andres, L. A., and Vance, J. M., "Measurements of Pressure Distributions and Force Coefficients in a Squeeze Film Damper Part II: Partially Sealed Configuration," *Tribology Transactions*, Vol. 34, No. 3, 1991, pp. 383–388.

[3] San Andres, L. A., "Effect of Fluid Inertia on Force Coefficients for the Long Squeeze Film Damper," *Tribology Transactions*, Vol. 31, No. 3, 1988, pp. 370–375.

[4] San Andres, L. A., and Vance, J. M., "Effect of Fluid Inertia on the Performance of Squeeze Film Damper Supported Rotors," *Journal of Engineering for Gas Turbines and Power*, Vol. 110, No. 1, 1988, pp. 51–57.

[5] San Andres, L. A., and Vance, J. M., "Effect of Fluid Inertia on Squeeze-Film Damper Forces for Small-Amplitude Circular-Centered Motions," *ASLE Transactions*, Vol. 30, No. 1, 1987, pp. 62–68.

[6] San Andres, L. A., and Vance, J. M., "Effect of Fluid Inertia and Turbulence on the Force Coefficients for Squeeze-Film Dampers," *Journal of Engineering for Gas Turbines and Power*, Vol. 108, No. 2, 1986, pp. 332–339.

[7] Tichy, J. A., "A Study of the Effect of Fluid Inertia and End Leakage in the Finite Squeeze Film Damper," *Journal of Tribology*, Vol. 109, No. 1, 1987, pp. 54–59.

[8] Tichy, J. A., "Effects of Fluid Inertia and Viscoelasiticity on the One-Dimensional Squeeze-Film Bearing," *ASLE Transactions*, Vol. 27, No. 2, 1984, pp. 164–167.

[9] Tichy, J. A., "Effects of Fluid Inertia and Viscoelasiticity on Squeeze-Film Bearing Forces," *ASLE Transactions*, Vol. 25, No. 1, 1982, pp. 125–132.

[10] Majumdar, A. K., "A Generalized Fluid System Simulation Program to Model Flow Distribution in Fluid Networks," SvT Rept. 331-201-96-003, Sverdrup Technology, Inc., Huntsville, AL, Oct. 1996.

[11] Vance, J. M., *Rotordynamics of Turbomachinery*, Wiley, New York, 1988, pp. 240–247.